Responsive Soft Interface Liquid Crystal Microfluidics

Ayşe Nurcan Özşahin and Emre Bukusoglu*

The multifunctional responsive interfaces of liquid crystal (LC) and water are employed in fundamental research (colloidal assembly) and promising applications (sensing, release, and material synthesis). The stagnant LC systems, however, limit their use in continuous, automated applications. A microfluidic platform is reported where stable LC flow is maintained between aqueous interfaces. The LC-water soft interface is defined by the preferential wetting of the two phases at the chemically heterogeneous microchannel interfaces. It is shown that the LC-water interfaces are stable up to significant pressure differences across the interfaces and maintain responsive characteristics. The stability is in a range to cover the perpendicular and flow-aligned regimes at low and high flow velocities, respectively, in co-current or counter-current flow configurations. The LC configuration at the vicinity of the aqueous interfaces is influenced by the shear induced by the bulk LC flow and by the contacting aqueous phases allowing modulation of the LC strain at the responsive interfaces. The simplicity of the construction and operation of the soft-interface LC flow platform shows promise and meets the fundamental requirements for their integration into next-generation autonomous platforms.

1. Introduction

Liquid crystals (LCs) are the delicate phases of matter that exhibit ordering at the mesoscopic scales, fluidic nature, and birefringent optical properties.[1,2] LCs have been developed as next-generation responsive materials that are suitable for label-free reporting of the changes occurring at their interfaces, on-demand release systems, anisotropic material synthesis platforms, and electro-optical devices, among others.[3–8] Most of the successful systems developed so far employed the multifunctional LC-water interfaces as a medium to facilitate i) the interaction of the mesogenic constituents of the LCs with the species present in the aqueous phase (for sensing purposes, material synthesis, and release activation), ii) the delivery of triggers induced or hosted by the aqueous phase (shear by flow or motile species) or iii) the delivery of the mobile species at the LC interfaces (small to macromolecules, nano-, and microparticles).[3–5,9,10] LC interfaces are delicate and respond to changes occurring at as low as nM to pM concentration and 1 Pa shear stress levels, which are challenging to measure with conventional methods.[2–4] Although promising results have been reported that can be transformed into useful functions, they were limited to the stagnant LC systems, in most cases limiting their use in continuous applications. While continuous, automated systems are of extreme importance in critical applications including disease control, early (marker-based) diagnostics, and environmental/public health control, which require high throughput periodic analysis and rapid action, the forward leap toward integration of LCs into flow systems is challenging due to the critical need for fundamental knowledge and design requirements for applications. The challenge starts with the stabilization of the LC underflow while accommodating "soft", fluidic, responsive interfaces for species exchange. In this study, we focus on establishing such requirements and present a platform that is open for future developments.

The LC-based systems differ from their isotropic counterparts through the three key concepts, namely surface anchoring, elasticity, and the formation of topological defects.[2,11–13] The LC director profiles within stagnant systems are usually explained by the minimization of the energy penalty caused by the contributions of such key concepts. The introduction of flow in confined LCs, however, results in significant changes to the states (configurations, director profiles, flow profiles) maintained in the stagnant LC medium.[14] The knowledge of the microflow of LCs is currently at a state of an understanding of the LC configurations with varying flows of the LC phases in channels with solid, homogenous, and "inactive" contacting surfaces that do not accommodate medium for species exchange.[14–20] Such studies, however, showed that the LC ordering within microchannels can be tuned via the flow velocity. These studies demonstrated a velocity-dependent LC configuration (and flow profiles).[15,17,19,21] At the weak flow regime, the LC elasticity was dominant and the distortions in director profiles were minimal. At the strong flow regime, the viscous forces dominate over the elasticity, and a flow-aligned state is maintained in the channels. However, in intermediate LC flows lies an unprecedented, delicate state of the

A. N. Özşahin, E. Bukusoglu
Department of Chemical Engineering
Middle East Technical University
Dumlupınar Bulvarı No.1 Çankaya, Ankara 06800, Türkiye
E-mail: emrebuk@metu.edu.tr

intermediate flow regime resulting from the backflow characteristic of the elastic fluids.[15] In non-uniform anchoring conditions at channel boundaries, or externally generated non-uniform ordering profiles (through phase transitions, electric fields, or sound waves), flow-dependent, useful defect structures have also been reported that were suitable for micro cargo concepts.[16,18,20–26] Recent studies also revealed the formation of flow-induced chiral configuration profiles (for example formation of flow-induced chiral states or distorted chiral director profiles).[24,27,28] Beyond these, the free interfaces of LC and water were also shown to be open to new explorations when the momentum, mass transfer, and elastic interactions were coupled.[5,29,30] Furthermore, the interfacial ordering profiles at such interfaces were revealed to play a critical role in colloidal interactions at interfaces.[31,32] Such observations support the delicacy of the system to minor changes which open ground for promising applications; thus, we seek to reveal the critical understanding required to proceed toward the next generation platforms as it necessitates the presence of the "soft", accessible interfaces that allow externally triggered interfacial anchoring transitions or externally induced interfacial shear to the flowing LCs.

Past examples of "soft" interface microfluidics include isotropic fluid flow within gas or immiscible liquid interfaces. Within these studies, multiple approaches including flow focusing, photolithography, contact angle pinning, and interfacial solid structuring approaches among others have been applied successfully to stabilize the fluidic interfaces during the flow of the substances within microchannels.[33–41] It is shown to be crucial to satisfy a well-defined solid channel boundary of hydrophobic-hydrophilic interfaces contacting the two phases of the fluids to stabilize the flow of the fluids within microchannels.[34,38] The phase boundary between the two fluids is stabilized by the Laplace pressure across the fluid interface.[33,36,37] The systems of interest among these studies are usually in the scales of 10—100 µm in depth. At these length scales the "soft" interfaces were shown to be stable up to pressures of 3 to 80 mbar for water-air interfaces and water-organic interfaces (for ≈200 and 10 µm-deep channels, respectively), where the advantage of the contact angle pinning at sharp edges w as also employed.[33,37,40] For LCs, the interplay between the elasticity (scales with ≈KL, where L is the length scale, typically $K = 10^{-11}$ N) and the interfacial anchoring (scales with ≈$W_A L^2$, typically $W_A = 10^{-3}–10^{-2}$ mJ m^{-2}) occurs in the order of $L = 10$ µm. Thus, the most promising application outcomes are usually revealed within the characteristic length scales ≈10 µm. Although the findings in the literature show promising stability of the soft interfaces, considering the delicacy of the "soft" interfaces and the necessity of the small-scale microfluidics, the success of similar approaches is not readily evident for LCs due to their wetting properties.[42,43] Furthermore, within these length scales of microchannels, the configuration states assumed as a function of the elasticity, interfacial anchoring, and the shear conditions within bulk or at the interfaces of the confining volumes have not yet been studied in flow systems and offer promising novel applications that are described above.

We seek to establish an LC-based, multiphase microfluidic platform where LC maintains pre-defined interfaces with the co-flowing aqueous interface to allow delivery of the additional species to the interfaces of the LCs. Within the context of this article, we study the formation a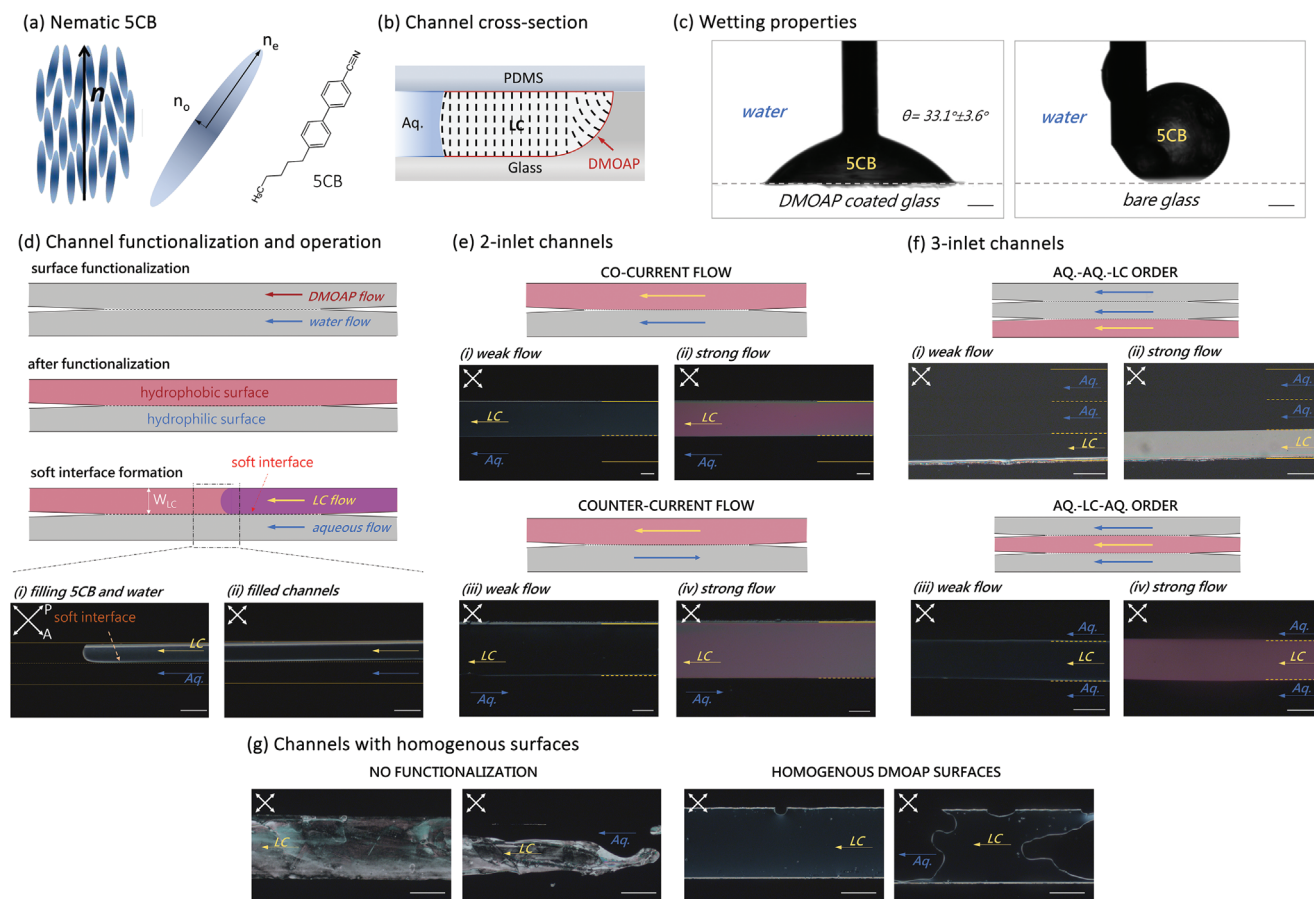nd stabilization of the LC-water "soft" interfaces in microfluidics and seek to provide a fundamental understanding of how varying shear and anchoring conditions at such interfaces influence the ordering characteristics within the LC phase under confinement. We also showcase the optical response of the LC phase to the changes in the chemistry of the LC-contacting interfaces. Such a platform does not only make possible the integration of LCs into continuous systems, but it also offers breakthroughs for further improvement on the capabilities of the LC-based responsive systems including autonomous devices.

2. Results and Discussion

2.1. Channel Fabrication and Stabilization of Liquid Crystal-Water Soft Interfaces

We employed a flow-focusing strategy to functionalize the inner surfaces of the microfluidic channels (typically 14 µm-deep) with two distinct wetting properties: hydrophobic and hydrophilic. We used DMOAP to treat the surfaces of the channels for the hydrophobic property, which is also known to induce homeotropic (perpendicular) orientation of 5CB (**Figure 1**a–c).[15] After microchannel fabrication steps were completed, we successfully coated one side of the channels in the longitudinal direction with DMOAP whereas the rest remained as a bare glass surface (Figure 1b,d) (details in the Experimental Section). After the inlet of 5CB along with an aqueous phase (from the right side of the image), we observed that the 5CB flow followed the DMOAP-coated interface spontaneously with no wetting of the bare glass interface, leading to the formation of an LC-water "soft" interface at the boundary of the DMOAP coated and bare interfaces (Figure 1d i,ii; Video S1; Figure S1, Supporting Information) (n > 20). We measured the static contact angle of the 5CB-pure water interface on DMOAP substrates as 33.1° ± 3.6° (n = 5) whereas we observed dewetting of 5CB at the interfaces with bare glass when submerged under water due to enhanced hydrophilicity (Figure 1c). Thus, the spontaneous formation of the stable LC-water interface corresponding to the DMOAP-bare glass/PDMS boundary was guided by the wetting of DMOAP interfaces by 5CB and the bare interfaces by the aqueous phase. Furthermore, we measured the static contact angles of the 5CB-air interface and water-air interface on both DMOAP-coated substrates and oxygen plasma-treated substrates. On DMOAP surfaces, we obtained the contact angles as 36.1° ± 3.8° (n = 10) and 87.0° ± 6.2° (n = 10) for 5CB and water, respectively. On oxygen-treated surfaces, we measured the contact angles as 16.6° ± 2.7° (n = 4) and 36.1° ± 3.7° (n = 4) for 5CB and water, respectively. As these measurements showed that 5CB wet on both surfaces, it was apparent that the wetting of water on the substrates had a decisive role in pre-determined pathways of the LC and aqueous phases since the notable difference in its wetting angles.

Under crossed polarizers with the orientations shown in Figure 1d i,ii, the dark appearance at the middle of the 5CB-side of the channel was consistent with the homeotropic anchoring of 5CB at the DMOAP coated surfaces (both top PDMS and bottom glass surfaces). The bright optical appearance at the hard (glass) side interface of 5CB was due to the strain caused by the homeotropic LC anchoring at the side walls. With such evidence

**ADVANCED
SCIENCE NEWS**

www.advancedsciencenews.com

**ADVANCED
MATERIALS
INTERFACES**
Open Access

www.advmatinterfaces.de

Figure 1. Flow of liquid crystals in soft interface microfluidic platforms. a) Schematic illustrations of the nematic ordering, birefringence of a representative LC molecule, and the molecular structure of 5CB, b) schematic illustration of the cross-section of a representative microfluidic channel and the LC configuration with the absence of (or weak) flow, c) images of a droplet of 5CB on DMOAP-coated (left) or bare glass (right) surfaces immersed in water, d) sketches of the surface functionalization procedures, the structure of the channel after functionalization, and the flow of LC and aqueous phases in the microfluidic channels. The polarized optical micrographs belong to i) the spontaneous filling of 5CB within the channel and ii) the filled channel with LC and aqueous phases. W_{LC} shows the width of the channel occupied by LC flow. e) Schematic illustration of the microfluidic channel named "2-inlet", having two inlets and outlets. Polarized optical micrographs show that both co-current and counter-current flows can occur in the channel, maintaining the soft interface. Both weak flow i, iii) and strong flow ii, v) cases of each flow configuration are shown. f) Schematic illustration of the microfluidic channel named "3-inlet", having three inlets and three outlets. Flow of two aqueous phases and LC were obtained in the arrangement of LC at one side close to the channel wall and LC at the middle. The polarized optical micrographs shown in the figures correspond to the weak i, iii) and the strong flow ii, iv) in the microfluidic channels. g) Polarized optical micrographs of LC and aqueous flow in a microfluidic channel with unmodified (left) and homogeneously DMOAP (right) coated surfaces showing the unsuccessful stabilization of LC-aqueous interface. The two double-sided arrows in optical micrographs show the directions of the analyzer and the polarizer filters. Scale bars: c) 400 µm, d–g) 100 µm.

and the planar anchoring of 5CB at the water interface, we concluded that the LC configuration within the channel cross section was consistent with the sketch of our initial expectation shown in Figure 1b. We also note that the LC appears bright at the soft interface. We found this bright appearance to be majorly due to the influence of shear induced by the aqueous flow at that interface (with a minor contribution of the curvature of the LC-water interface) which we explain further below.

The LC-water interface was durable enough during flow that it was stable up to pressures of >200 mbar applied equally to the two phases at their inlets. At such increased pressures, we observed that the LC ordering was strained to possess a tilted alignment (bend distortions) in the direction of flow, which has been previously referred to as a "strong" flow. Such a configuration is evidenced by the transition from the dark, homeotropic state at

low velocities to the bright, deformed state under crossed polarizers at high velocities as shown in Figure 1e from i (weak flow) to ii (strong flow).

In addition to the co-current flow configuration of LC and aqueous phases, the LC-water interface was stable to maintain a counter-current flow configuration. With such a flow configuration, we observed the weak and strong flow configurations can also be maintained as shown in Figure 1e iii,iv, respectively, as evidenced by the appearance of a bright, birefringent region at the middle of the 5CB side. Considering the local pressure distribution of the two distinct phases within the channel, such a flow configuration corresponded to a variation in the pressure differences across the LC-water interface ($\Delta P_{int} = P_{Aq} - P_{LC}$) along the flow direction. The local ΔP_{int} ranges from negative to positive values that showed the significant stability of the

LC-aqueous interface against net forces in the two opposite directions of the interface normal. We detail this phenomenon below after further characterizations of the stability of the LC-water microfluidic interface.

The LC flow geometry was not limited to the channels with two inlets. We were successful in the operation of the channels with three independent inlets as shown in Figure 1f. With this geometry, the LC flow can be maintained in flow rates covering the weak and strong flow configurations in channels where the LC was flowing at one side of the channel (LC-Aq.-Aq. order, Figure 1f i,ii) and where the LC was flowing between two aqueous phases (Aq.-LC-Aq. order, Figure 1f iii,iv) (Video S2, Supporting Information). Such geometrical flexibility is useful in terms of generating i) two aqueous phases that can be used for analytical purposes such as analyte, reference, and buffer flows among other further application-related purposes, thus, showing the promising evidence for further improvements of such a platform, ii) two LC-water interfaces that can be manipulated by two independent flows of water.

We note that the stable LC flow was possible only when the two distinct (hydrophilic and hydrophobic) functionalities of the glass surfaces were present within the channel. When bare glass surfaces or homogenous DMOAP surfaces were used, we observed unsuccessful stabilization of the LC-water interface during flow. With such homogenous interfaces (either bare or DMOAP-coated), we observed the formation of 5CB (or water) droplets or sequential slugs of LC and aqueous phase during flow operation as shown in the representative micrographs in Figure 1g (Videos S3a,b and S4, Supporting Information for more detailed results).

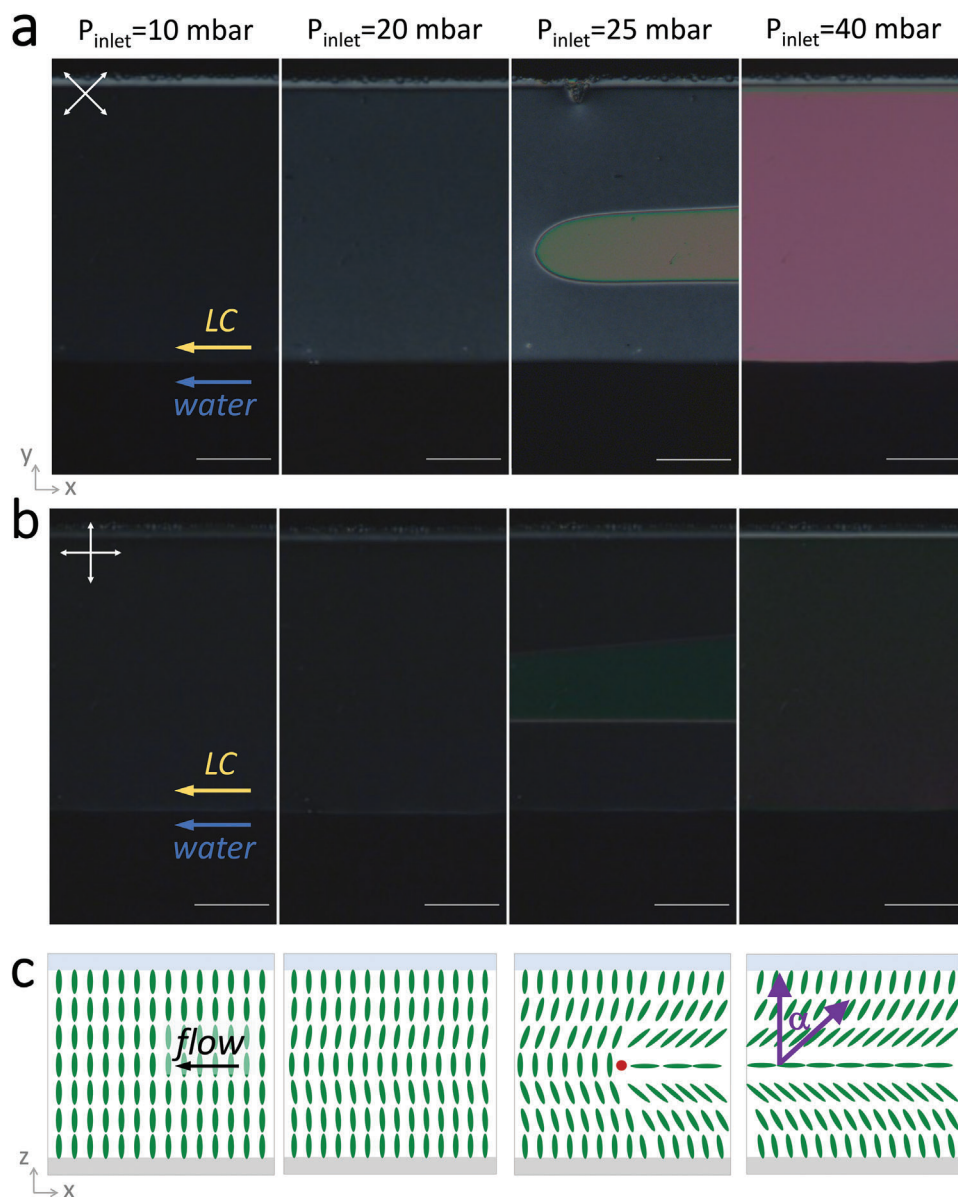## 2.2. Characterization of the Flow of Liquid Crystals Maintaining Soft Interfaces

The flow-induced alignment of the LC phase is shown in **Figure 2** where the polarized optical micrographs were taken at a range of equal inlet pressures of the LC ($P_{LC,inlet}$) and aqueous ($P_{Aq.,inlet}$) phases, which we define both as "P_{inlet}". At low pressures, we observed complete dark appearances of the LC phase (e.g.: $P_{inlet} = 10$ mbar case) at the two orientations of the analyzer and polarizers (Figure 2a,b and detailed in Figure S2, Supporting Information). This indicated that the LC orientation was perpendicular to the imaging plane uniformly through the depth of the channel. At these conditions, we measured the average velocity of the LC (v_{LC}) to be ≈15 μm s^{-1}. When the pressure was increased to 20 mbar ($v_{LC} \approx 20$ μm s^{-1}), although the appearance of the LC side was still dark, we observed an increase in the intensity of the transmitted light (compared to the case of $P_{inlet} = 10$ mbar) when the analyzer and the polarizer were oriented 45° and 135°, respectively. This increase in the intensity, with the absence of such an appearance when the LC was imaged at 0° and 90° orientation of the analyzer and the polarizer, suggested a distortion of the LC configuration along the direction of the flow. Increasing the inlet pressures further resulted in an increased transmitted light intensity when the analyzer and the polarizer were oriented at 45° and 135°, respectively. This increase further resulted in an evident change in the optical appearance of the LC phase under the polarized optical microscope as shown in the

case of $P_{inlet} = 25$ mbar which is referred to as an ordering transition. Such a transition was reported by Čopar et al.[19] Sengupta et al.[15] and Emeršič et al.[18] previously, which was characterized by the formation of a defect front that moves with the flow and results in a bright, birefringent optical appearance of the LC phase (the sketch of this transition structure and the defect as a red dot are shown in Figure 2c). Observation of such a transition, with no significant change in the optical appearance of the LC phase at 0° and 90° orientation of the analyzer and the polarizer suggested the formation of the "dowser" (or "horizontal") state from the initially distorted "bowser" (or "vertical") state.[15,17–19,44] These configuration states induced by the flow are characterized by the orientation of the nematic director at the half depth of the channel perpendicular to the imaging plane in the vertical ("bowser") state whereas the horizontally aligned counterpart is the "dowser" state. We measured the critical v_{LC} to induce such transition as ≈80 μm s^{-1} for ≈14 μm-deep channels (n = 6) by velocity measurements of the particles dispersed in the LC phase. Such a critical velocity for the transition is consistent with past reports that investigate the flow-induced transitions in hard-interface microfluidic channels with similar thickness.[15,19] When the transition to the "dowser" state occurred, we observed a uniform birefringence color within the 5CB phase confirming the maintained "dowser" state. Representative micrographs of this configuration at two orientations of the analyzer and polarizer are given for the flow condition of $P_{inlet} = 40$ mbar are given in Figure 2a,b. At these conditions, we measure $v_{LC} = \approx100$ μm s^{-1}. We estimated the tilting angle (α) to be ≈50° using the birefringence coloring in Figure 2a and the retardation values from the Michel–Levy chart using the methods described in the literature (A similar experiment is also shown in Video S5, Supporting Information for a 3-inlet channel.).[45]

2.3. Stability of the Liquid Crystal-Aqueous Soft Interfaces

To provide more insight into the stability of the LC-water interface and the ordering of LCs at its vicinity, we performed experiments with unequal inlet pressures of the aqueous and LC phases of the 2-inlet channels. Such an experiment was motivated by the observation of the stability of the LC-water interface in multiple flow configurations leading to special variations in ΔP_{int} as described in Figure 1. In such experiments, we kept the pressure at the inlet of the LC phase constant (as $P_{LC,inlet} = 23$ mbar in **Figure 3**) and varied the pressure at the inlet of the aqueous phase ($P_{Aq.,inlet}$) while imaging the LC flow with polarized optical microscopy. A representative experiment shown in Figure 3 revealed that the dark appearance at the middle region of the LC phase (away from the interfaces) remained unchanged with increased $P_{Aq.,inlet}$, supporting $P_{LC,inlet}$ driven flow at the bulk of the LC side. However, we observed the brightness of the interface to increase with increased $P_{Aq.,inlet}$, when the analyzer and the polarizer were oriented 45° and 135°, respectively (intensity plots are shown as insets in Figure 3a). The increase of the intensity at the interface was monotonous as shown in the insets of Figure 3a, which was consistent with the bend distortions of the LC director field along the flow direction (equivalent to the bulk distortions presented in Figure 2). Figure 3b shows such representative sketches of the LC director configurations at the midplane (at z = h 2^{-1}, where h is

**ADVANCED
SCIENCE NEWS**

www.advancedsciencenews.com

**ADVANCED
MATERIALS
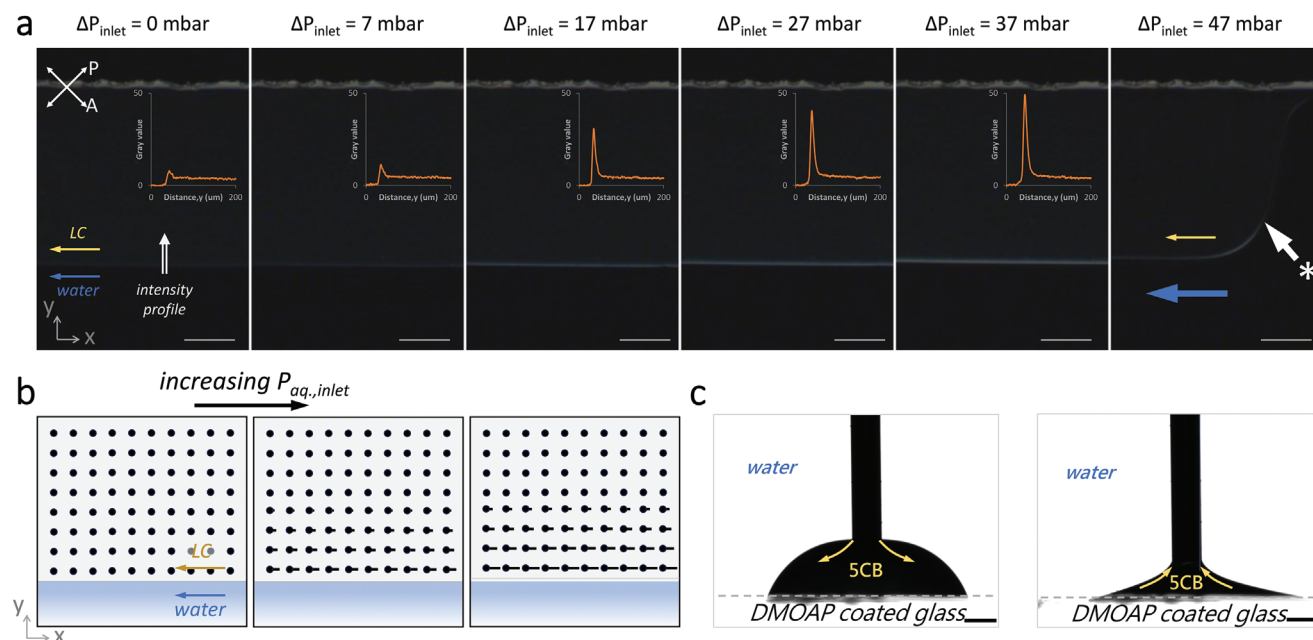INTERFACES**
Open Access

www.advmatinterfaces.de

Figure 2. Flow-induced configurations of 5CB within microfluidic channels with soft interfaces. Optical micrographs of 5CB flowing within the microfluidic channels at the indicated, equal inlet pressures of 5CB and the aqueous phases. Polarized optical micrographs in a) were collected when the analyzer and the polarizer were oriented 45° and 135°, respectively, and in b) were collected when the analyzer and the polarizer were oriented 0° and 90°, respectively. Scale bars: 100 μm. c) Example sketches for the alignment maintained in the channels determined from polarized optical microscopy images.

the channel depth) of the microfluidic channels corresponding to the increased $P_{Aq.,inlet}$ as we evidenced from such polarized optical microscopy characterizations (Similar shear experiment with a 3-inlet channel in Aq.-LC-Aq. order is shown in Video S6, Supporting Information).

We observed the LC-water interface to be stable within a significant range of pressure differences across that interface, which we define as $\Delta P_{inlet} = P_{Aq.,inlet} - P_{LC,inlet}$. In experiments, we measured a maximum ΔP_{inlet} (ΔP_{max}) where the LC-water interface ruptures and no longer be possible to maintain a stable co-flow of LC and the aqueous phase. An example of this rupturing

process is shown in Figure 3a which occurred at $\Delta P_{inlet} \approx 47$ mbar (the ruptured interface is shown with a white asterisk). With independent experiments, we measured $\Delta P_{max} = 40.5 \pm 7.2$ mbar (n = 10). Similarly, we measured the ΔP_{max} for the case where the $P_{LC,inlet}$ was higher than the $P_{Aq.,inlet}$ as $\Delta P_{max} = -31.9 \pm 9.3$ mbar (n = 6) by keeping the $P_{Aq.,inlet}$ constant and varying the $P_{LC,inlet}$ in such experiments.

For soft interface microfluidic flow systems (either organic–water or water–air interfaces), the literature suggests the Laplace pressure at such soft interface to be responsible for the interface stabilizations.[33,34,36] The Young-Laplace equation for a

2400334 (5 of 13)

**ADVANCED
SCIENCE NEWS**

www.advancedsciencenews.com

**ADVANCED
MATERIALS
INTERFACES**
Open Access

www.advmatinterfaces.de

Figure 3. Stability and the structure of the LC-water soft interfaces. a) Polarized optical micrographs of 5CB flowing within the microfluidic channels at the indicated pressure differences across the 5CB and the aqueous phases ($P_{5CB,inlet}$ = 23 mbar kept constant). Orange inset graphs show the intensity profiles of the interfacial regions determined from each micrograph in the direction of the white arrow labeled as "intensity profile". Scale bars: 100 μm. b) Representative sketches of the LC configurations maintained at the midplane of the microfluidic channels upon increasing interfacial shear via increasing $P_{Aq.,inlet}$. c) Photographs of a droplet of 5CB on DMOAP-coated surfaces immersed in water were taken during measurements of the advancing and receding contact angles. Scale bars: 500 μm.

cylindrical LC-water interface (considering the conceptual equivalency of our microfluidic LC-water interface) is;

$$\Delta P = \gamma / R_{int} \tag{1}$$

where γ is the interfacial tension at the LC-aqueous interface (30.4 ± 0.1 mN m^{-1}, n = 3) and R_{int} is the radius of curvature of the same interface. The maximum pressure that the soft interface in the same geometry can sustain then becomes;
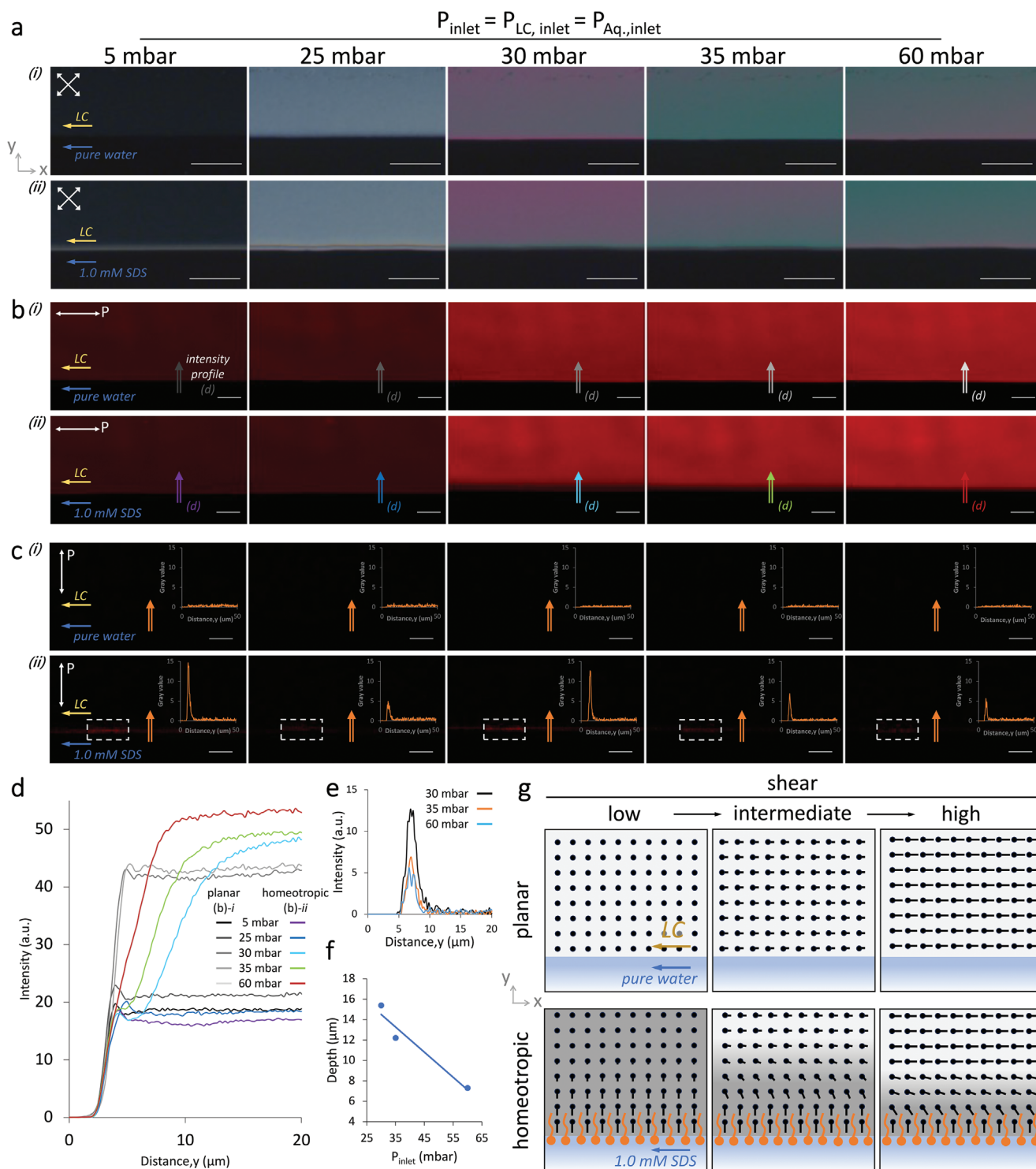
$$\Delta P_{max} = (2\gamma / h) \sin\left(90° - \theta_{LC-Aq.}\right) \tag{2}$$

where $\theta_{LC-Aq.}$ is the contact angle of the LC-water interface at the solid interfaces. Such a discussion has also been extended to the cases of the moving liquid interfaces (advancing or receding contact angles).[37] We measured the advancing and receding contact angles of 5CB on DMOAP-coated glass interfaces in water to be θ_{adv} = 64.6° ± 4.7°, and θ_{rec} = 19.4° ± 4.7° (n = 4), respectively (Figure 3c). Using these measured values, we calculated the ΔP_{max} for positive ΔP_{inlet} (where $P_{Aq.} > P_{LC}$) and negative ΔP_{inlet} (where $P_{Aq.} < P_{LC}$) cases to be 40.8 ± 1.2 mbar and −18.6 ± 3.2 mbar, respectively, for h = 14 μm. Such calculations were in good agreement with our measurements of the stability of the LC-water interfaces reported above. We reasoned the higher stability in the case of $P_{Aq.} < P_{LC}$ in our experiments to be due to the contact angle pinning effect at the DMOAP-bare glass interfaces during rupturing of the LC-Aq. interface. We also measured ΔP_{max} for ≈20 μm-deep channels to be 31.3 ± 5.8 mbar (n = 3), which was in parallel with the predictions of Equation 2. When a common surfactant, sodium dodecyl sulfate (SDS) was

added to the aqueous phase stream, we measured the interfacial tension to reduce to 19.5 ± 0.3 mN m^{-1} (n = 3) at 1 mM concentration and the θ_{adv} = 58.9° ± 4.6°, and θ_{rec} = 12.5° ± 0.3° (n = 3), respectively. As predicted by Equation 2, ΔP_{max} for such an interface would reduce linearly with the interfacial tension to a value of 27.2 ± 0.5 mbar. Our experimental measurements of 1 mM SDS water-5CB interfaces revealed a ΔP_{max} of 29.6 ± 5.7 mbar (n = 4), consistent with the predictions.

2.4. Response of the Liquid Crystal-Aqueous Soft Interfaces Against Shear and Molecular Adsorption

Figure 4a shows the polarized optical micrographs of a 14 μm-deep channel where 5CB (0.01% Nile Red doped, reasoned below) was flowing in contact with either pure water (top, i) or 1.0 mM SDS solutions (bottom, ii) at equal inlet pressures of LC and aqueous phases as indicated. 1.0 mM SDS is known to induce a homeotropic anchoring of 5CB at the initial planar alignment at their interfaces of the pure aqueous phases.[46] When comparing the two cases shown in Figure 4a i,ii, it is evident that the bulk of the LC phase was not influenced by the composition of the contacting aqueous phase. However, when the optical appearances of the two interfaces were compared, the bright optical appearance of the LC-1.0 mM SDS interface was visible (bright) (n > 20) when the analyzer and the polarizer were oriented 45° and 135°, respectively. Polarized optical micrographs with cross polarizers oriented at 0° and 90° revealed a bright appearance at the LC-1.0 mM SDS interface due to the strain caused by the homeotropic anchoring, but a dark appearance was maintained

ADVANCED
SCIENCE NEWS

www.advancedsciencenews.com

ADVANCED
MATERIALS
INTERFACES
Open Access

www.advmatinterfaces.de

Figure 4. The structure of the LC-water soft interfaces. a) Polarized optical micrographs of 5CB flowing within the microfluidic channels at the indicated inlet pressures of 5CB and the aqueous phases ($P_{5CB,inlet} = P_{Aq.,inlet}$) of i) pure water (planar anchoring) and ii) 1.0 mM SDS (homeotropic anchoring) solutions. Fluorescent confocal polarized micrographs collected at b) 0° and c) 90° polarization of the excitation light for channels with 5CB flowing within the microfluidic channels while contacting with i) pure water (planar anchoring) and ii) 1.0 mM SDS (homeotropic anchoring) solutions. The colored arrows in micrographs show the direction of the intensity profile plotted in d) with the indicated coloring. Orange inset graphs in (c) show the intensity profile for each micrograph in the direction of the orange arrow labeled as "intensity profile". The inset images in dashed lines show the same location of the image with 50% increased brightness to indicate the interface brightness. Scale bars: 100 µm. e) The intensity profiles for 30, 35, and 60 mbar cases in (c) drawn for comparison. f) The depth of the interfacial region measured from images in (b-ii) with respect to P_{inlet}. g) Representative sketches of the LC configurations maintained at the midplane (h/2) of the microfluidic channels for the two anchoring conditions at the LC-aqueous interface upon increasing bulk shear.

**ADVANCED
SCIENCE NEWS**

www.advancedsciencenews.com

**ADVANCED
MATERIALS
INTERFACES**
Open Access

www.advmatinterfaces.de

in the bulk LC phase (detailed micrographs available in Figure S3a,d, Supporting Information for planar and homeotropic case, respectively). In addition, at higher flow rates, the difference in the optical appearance of the interface when compared to the bulk was evident in the 1.0 mᴍ SDS case. Such an optical appearance supports the homeotropic anchoring of 5CB at the interface of 1.0 mᴍ SDS. Consistent with the maintained tilting of 5CB at the LC-aqueous interfaces, we observed an SDS concentration-dependent optical appearance in polarized micrographs at intermediate SDS concentrations (0.1 and 0.5 mᴍ) as shown in Figure S3b,c (Supporting Information).

The fluorescence confocal polarized micrographs (FCPM) of the mid planes of the channels (h/2) of 0.01% Nile Red dye doped 5CB at polarizations of either 0° and 90° are shown in Figure 4b,c, respectively. The Nile Red fluorophore is known to align parallel to the local director of 5CB and possesses a polarization-dependent absorption spectrum of the excitation light showing maximum when the polarization direction and the molecular director are parallel to each other. Thus, FCPM allows the determination of the local director orientation of the LC nematogens.[47] While analyzing the FCPM micrographs at 0° polarization of the fluorescence excitation light, we did not observe a significant difference between the optical appearances of the pure water and 1.0 mᴍ SDS cases within the flow rates corresponding to the weak flow regime (compare images in Figure 4b up to 25 mbar). Such similarity was not surprising as neither shear nor the SDS-induced interfacial alignment was expected to result in a net orientation of 5CB in the direction of the 0° polarization of excitation light. However, within these flow rates, the higher intensity of the LC-water interface of the 1.0 mᴍ SDS case was evident when the polarization of the excitation light was 90°, which was absent in the case of the pure water (Figure 4c, images and inset intensity plots). Consistently, we observed the interfacial alignment of 5CB at aqueous interfaces to assume an orientation closer to the homeotropic state as SDS concentration was increased (Figure S3a–d iii, Supporting Information shows detailed images for pure water, 0.1, 0.5, and 1 mᴍ SDS cases).

When the micrographs corresponding to the strong flow were analyzed ($P_{inlet} \geq 30$ mbar), the increased brightness within the 5CB phase was evident as shown in Figure 4b i. In these images, we observe no significant change in the distribution of the brightness within the 5CB phase, while the interface was slightly brighter than the bulk of the 5CB. Such observations were consistent with the planar anchoring at the aqueous interface and the shear-induced alignment of LCs toward the direction of flow as sketched in Figure 4d. When the micrographs of 5CB contacting with 1.0 mᴍ SDS solution corresponding to the strong flow were analyzed (Figure 4b ii, $P_{inlet} \geq 30$ mbar), the intensities at the bulk of the 5CB phase (away from the interface) did not appear to be different from the planar anchoring case shown in Figure 4b i, revealing no influence of the interfacial conditions to the bulk flow away from the soft interface. However, when the intensities of the interfaces were examined, the dark appearance of the interfaces was evident when compared to the bulk. Moreover, the intensity of the homeotropic interface of strong flow is similar to the intensity of the same interface of the weak flow ($P_{inlet} \leq 25$ mbar) as also shown in Figure 4d. Consistently, the higher intensity of the LC-aqueous interface of the 1.0 mᴍ SDS case when $P_{inlet} \geq 30$ mbar was evident when the polarization of the ex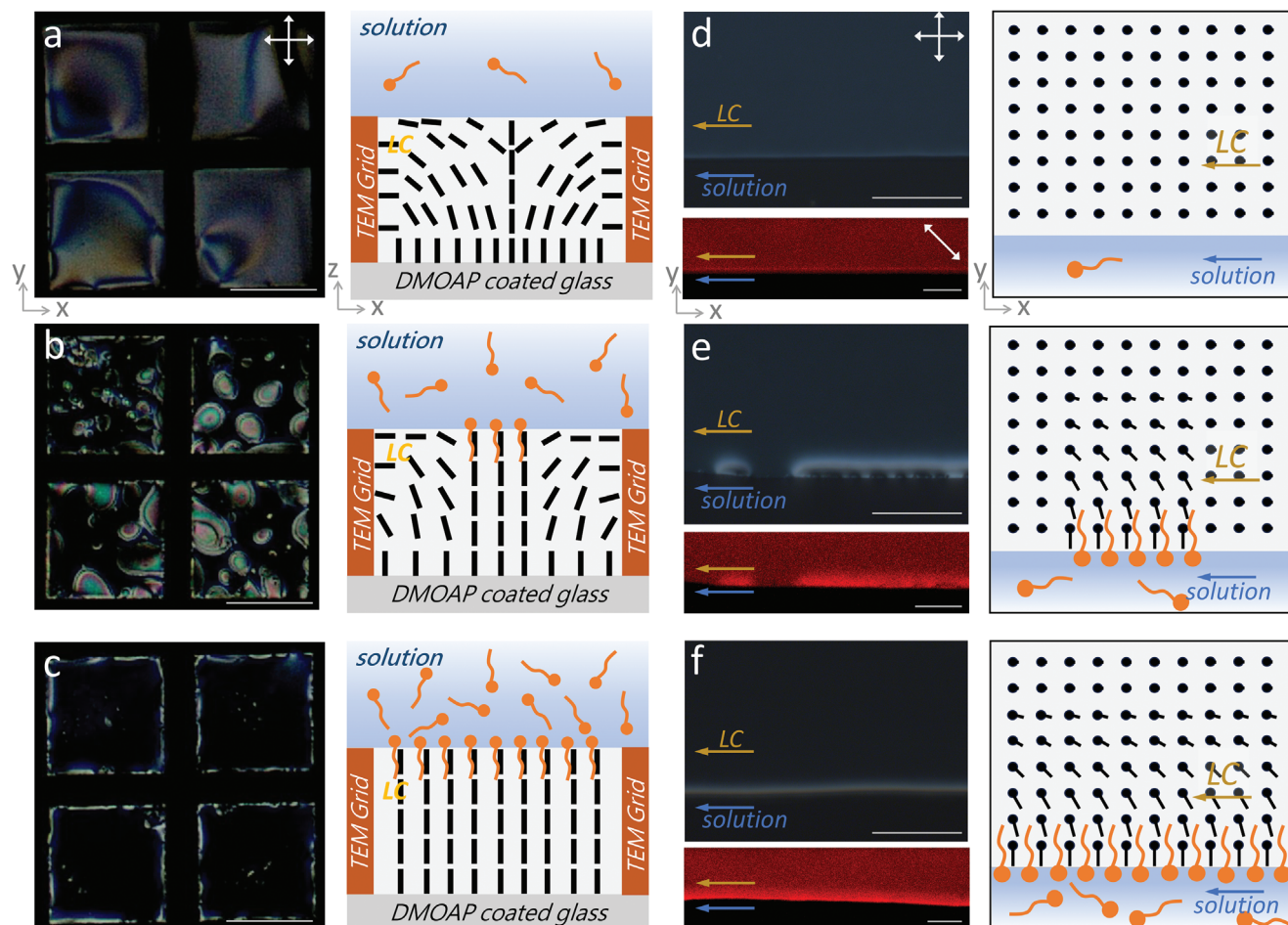citation light was perpendicular to the LC-aqueous interface (90°), which was absent in the case of the pure water (Figure 4c). At intermediate concentrations of SDS, we observed darker interfacial region as the interfacial tilting of 5CB approached to the homeotropic alignment (Figure S3a–d, Supporting Information).

From the intensity distribution at the vicinity of the interface, we measured the width of the "interfacial region" to be 15.4 μm for the flow induced by $P_{inlet} = 30$ mbar. We observed the width of this interfacial region to shrink to dimensions of 12.2 μm for $P_{inlet} = 35$ mbar and 7.3 μm for $P_{inlet} = 60$ mbar. This shrinkage was reasoned to be resulting from the coupling of the shear-induced (bulk flow of 5CB) distortions within the director field of 5CB and the strain caused by the anchoring conditions at the interfaces of aqueous SDS and DMOAP interfaces. With such observations, we concluded that the anchoring, and flow-induced configuration regimes differ at the vicinity of the interfaces. With such evidence, we determined that the shear and interfacial anchoring-induced configurations maintained within the channels as sketched in Figure 4g. Consistent with this depiction, we observed that the intensity of the "interfacial region" was decreased when 5CB flow was imaged with FCPM at 90° polarization as shown with the inset diagrams sketched in Figure 4c, $P_{inlet} = 30$–60 mbar (also shown in Figure 4e). Moreover, we found a linear dependency between the shear induced by flow and the width of the interfacial region as shown in Figure 4f. Such linear dependency originated from the competition between the elastic force that scales with KL and the force induced by shearing of the LC phase with the pressure-driven flow.

The anionic surfactant SDS is known to result in heterogeneous interfacial phases when the adsorption occurs with the presence of simple salts due to the screening of the electrical double layers and the elastic attraction caused by the LC phase.[30,48] Observing the surfactant adsorption-induced ordering transitions at the LC-water interfaces, we examined the response of our "soft" interfaces of the microfluidic system to the heterogeneous interfacial species. After confirming the formation of phase-separated surfactant-rich and surfactant-lean phases at the LC-aqueous interfaces after equilibration of 5CB interfaces in contact with solutions of SDS and NaBr with a well-established system of TEM-grid supported 5CB films (**Figure 5**a–c, showing planar, heterogenous, and homeotropic interfaces of 5CB-aqueous phase, respectively), we performed experiments with our microfluidic channels. Figure 5d–f shows the polarized optical micrographs and FCPM images of such an experiment performed using 20 μm-deep channels (n = 3), where the aqueous phases were chosen to maintain planar, heterogenous, and homeotropic interfaces, respectively. As seen from the distinct heterogeneous distribution of the transmitted light intensity at the LC-aqueous interface of the channel in Figure 5e, the interfacial heterogeneity can be tracked with the soft microfluidic interfaces. The bright regions at the heterogenous interfaces were consistent with the intensity observed in the homeotropic interface case shown in Figure 5f, whereas the dark regions were consistent with the dark appearance observed in planar interfaces. Thus, the configuration of 5CB at the vicinity of the LC-aqueous interface can be depicted as sketched in Figure 5f.

We lastly comment on the two conceptual experiments that provide insight into the stability of the LC-aqueous "soft" interface of our microfluidic channel. First, as briefly introduced in
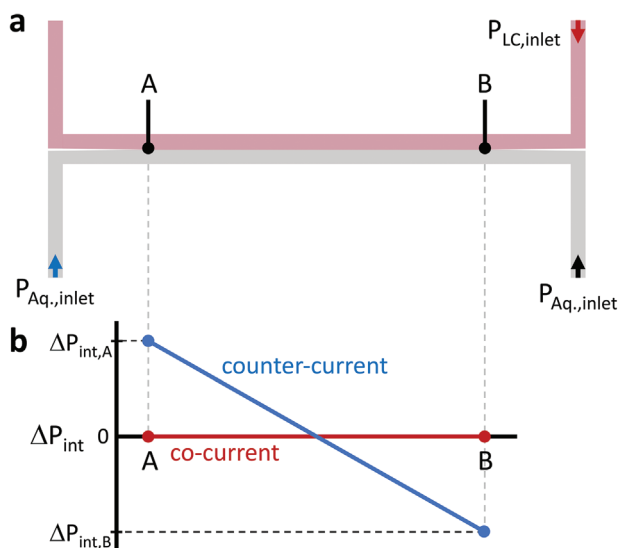
ADVANCED
SCIENCE NEWS
www.advancedsciencenews.com

**ADVANCED
MATERIALS
INTERFACES**
Open Access
www.advmatinterfaces.de

Figure 5. Imaging heterogenous LC-aqueous interfaces during flow. Polarized optical micrographs of a film of 5CB stabilized with a 25 µm-thick TEM grid equilibrated with a) pure water, b) a solution of 0.023 mM SDS and 1.0 mM NaBr, and c) 1.0 mM SDS solution, respectively. The representative sketches of the director configuration in the film 5CB are also shown adjacent to the related images. Polarized optical micrographs (top) and FCPM images (bottom) of 5CB in contact with d) 0.005 mM SDS in 1.0 mM NaBr, e) 0.015 mM SDS in 1.0 mM NaBr solution, and f) 1.0 mM SDS solution flowing within the microfluidic channels. The representative sketch of the LC configurations maintained at the midplane (h/2) of the microfluidic channels imaged in (d–f). Scale bars: (a,b,c) 100 µm, (d,e,f) 50 µm for POM images and 20 µm for FCPM images.

Figure 1, it was possible to stabilize the LC-aqueous interface in a counter-current flow configuration. We showed in Figure 1e that the weak and strong flow configurations can be established in such configurations. Although the LC-aqueous interface was stable in such a range of pressures that are promising for potential applications, we found that the interface was destabilized when the inlet pressures were above 35 mbar, however, such was not the case for co-current flow systems. We explain the reason for such observation using the sketch shown in **Figure 6**. As depicted in Figure 6b for a rough channel sketch in Figure 6a, the ΔP_{int} of the countercurrent flow configuration is a strong function of location, leading to its maximum absolute values at the interface where LC and aqueous phases form their first contact. However, such a location dependency is not expected in the case of the co-current flow configuration. Thus, although such a maximum limit does not exist for the co-current flow configurations within the conditions we performed experimentally, we were able to determine maximum P_{inlet} values for the microchannels with counter-current flow configurations. We estimate the

$\Delta P_{int,A}$ and $\Delta P_{int,B}$ for the case of $P_{inlet} = 36.7 \pm 6.2$ mbar to be 12.2 and -12.2 mbar (n = 3) in experiments, which are close to the ΔP_{max} values we measured experimentally for the case $P_{LC} > P_{Aq.}$ (Figure 3). Consistent with this, we observed the interface to destabilize first at point B indicated in Figure 6. Thus, such inlet pressures of the countercurrent result in destabilization of the LC-aqueous interfaces due to non-uniform distribution of ΔP_{int}, when the flow is in the countercurrent direction.

We conclude this article by commenting on the importance of the surface functionalization step on the stability of the LC-aqueous interface with the second conceptual experiment. In a typical channel functionalization step, the DMOAP solution was introduced into the channel at high flow rates (at $P_{inlet} = 150$ mbar) to minimize the diffusion of the DMOAP molecules to the pure water side, thus, maintaining a sharp transition from DMOAP-coated to the bare glass/PDMS surfaces within the channel. However, we found that when the DMOAP-coating was performed at lower flow rates (corresponding to the increased effect of side diffusion of DMOAP during coating), the

**ADVANCED
SCIENCE NEWS**

www.advancedsciencenews.com

**ADVANCED
MATERIALS
INTERFACES**

www.advmatinterfaces.de

Figure 6. Representative sketches of flow configurations. a) The two configurations of the microfluidic flow configurations. b) The variation of the ΔP_{int} along the LC-aqueous "soft" interface for the two flow configurations.

stability of the interfaces was influenced negatively, and the interfaces were no longer able to withstand after the introduction of surfactant-doped aqueous solution (Video S7, Supporting Information). Thus, maintaining a sharp transition from DMOAP-coating to bare interfaces is critical in the proper operation of the above-described LC flow systems.

3. Conclusions

We fabricated a microfluidic platform where the LC phase maintained a stable LC-aqueous soft interface during flow. We note that we have not developed a system specifically for direct application in this study; rather, we introduced a concept that will enable automation and open a pave for the development of the LC-based applications or final use. Such a system was not evident with the current state of the literature and was not trivial. Thus, we demonstrated the stability and the response of the LC-aqueous interfaces upon variations in the bulk shear introduced by the Poiseuille flow, interfacial shear introduced by the contacting aqueous phase, anchoring conditions, and interfacial tension caused by the surfactants present in the aqueous phase. Our study revealed that such a microfluidic platform was stable within useful flow rates of the LCs and water to induce ordering transitions (either leading to homogenous or heterogenous interfaces) and strained LC ordering at the vicinity of the LC-aqueous interfaces. There are no existing microfluidic flow systems that allow manipulating the flow on the LC side to change directly the LC state in a multi-phase microfluidic system, as demonstrated in this study. We underlined the impact of flow-dependent changes in this system related to the strain effect. Combining these observations with the recent literature on the enhanced response of such strained interfaces[49] along with novel applications resulting from the strained states of the LCs,[4,5,31,50] we concluded that the observations we reported here possess promising opportunities for future developments toward novel applications of LCs in-

cluding high-throughput analytical platforms, early-detection of the rare or critical diseases, continuous tracking advanced release platforms and interfacial synthesis of 2D self-assembled materials among others. In this context, the following examples illustrate potential future advances: i) understanding of the influence of the interfacial shear on the flow characteristics of the LC phase, ii) the characterization of the effect of the soft interface on the flow of complex fluids in microfluidic multi-phase channels, iii) manipulation of flow by altering the local ordering of LC within the microchannels through modification of surface properties, iv) observation of interfacial organization of amphiphilic species at LC-aqueous interfaces and the related anisotropic ordering of the bulk LC phase. Future research efforts will also benefit from the precise control of the strain profiles and understanding the response characteristics of such multifunctional interfaces that were coupled with the shear. Such attempts will lead to unique functional properties and applications of the LC soft interface microfluidic platforms.

We also lastly comment that the stability limit of the LC-aqueous interface against pressure differences was inversely dependent on the depth of the microfluidic channel. Thus, it would be challenging, at least with the same methods we propose here, to maintain a stable soft interface for deeper channels. This may not be an issue if the microfluidic platform is to be designed for sensor application as the confinement of the LCs is required in the size scales of 10 μm. However, improvements in the stability will be a necessity for some future developments.

4. Experimental Section

Materials: Glass slides were purchased from Marienfeld (Lauda–Königshofen, Germany), isopropyl alcohol was purchased from Isolab (Eschau, Germany), acetone (HPLC grade, 99.99%), octyltrichlorosilane (OTS), hexamethyldisilazane (HMDS), dimethyloctadecyl[3-(trimethoxysilyl)propyl]ammonium chloride (DMOAP) solution, sodium dodecyl sulfate (SDS), sodium bromide and Nile Red dye were purchased from Sigma–Aldrich (Steinheim, Germany), the positive photoresist AZP4620, AZ400K Dev 1:4 and AZ EBR solvent was purchased from Microchemicals (Ulm, Germany), BOE 7:1 was purchased from TECH-NIC Micropur (Saint–Denis, France), Sylgard 184 silicone elastomer kit was purchased from Dow Europe GmbH (Wiesbaden, Germany), 4-Cyano-4-pentylbiphenyl was purchased from Jiangsu Hecheng Chemical Materials Co. Ltd. (Jiangsu, China), and deionized water (18.2 MΩ cm) were used during the conducted experiments.

Microchannel Fabrication: The flow device consisted of a channel-etched glass slide and a flat polydimethylsiloxane (PDMS) part. The channel geometry (either two inlet and outlets (2-inlet) or three inlets and outlets (3-inlet) was obtained with lithography and wet-etching (BOE), on the glass slide as summarized in **Scheme 1**. The glass slides were first rinsed with acetone, pure water, and isopropyl alcohol and then dried. Then, HMDS was deposited for 5 min at 150 °C under vacuum to mediate the required hydrophobicity for photoresist adhesion (the photoresist was peeled off otherwise during wet etching). The positive photoresist AZP4620, which was diluted with AZ EBR solvent in a 1:1 ratio, was spin-coated on the glass substrate using a spin coater (Polos Spin 150i, Putten, The Netherlands). The coating was performed at a constant speed of 1000 rpm for 50 s, and the speeding up and down parts with a linear acceleration for 10 s each. A soft baking step at 110 °C on the hot plate for 50 s was applied after the spin-coating. Then, the glass was cooled down at room conditions and equilibrated for 10 min at room temperature. A maskless photolithography system, Polos NanoWriter equipped with a 405 nm laser was used to transfer the microchannel drawing onto

(a) Photoresist coating

HMDS coated glass
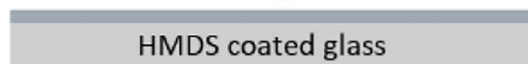
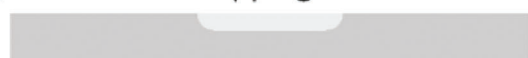## (b) Maskless photolithography

(c) Developing

(d) Wet etching
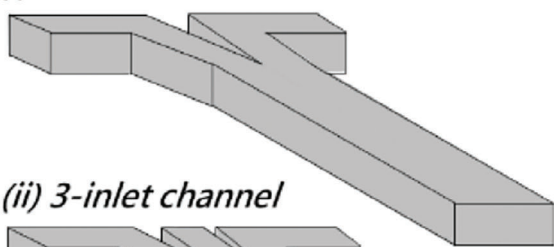
BOE

(e) Photoresist stripping
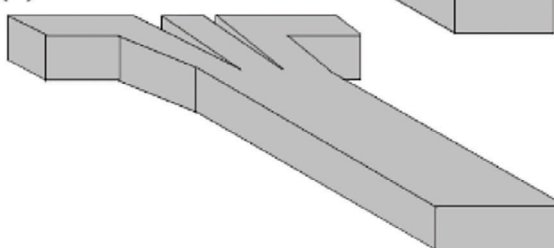
(f) PDMS bonding

(g) Channel geometries

(i) 2-inlet channel

(ii) 3-inlet channel

Scheme 1. The microfabrication of the microfluidic channels. The sketch shows the microfabrication steps of the microfluidic channels: a) spin coating of the photoresist on HMDS-coated glass slides, b) photolithography of the microchannels on photoresists, c) developing, d) wet etching with 7:1 buffered oxide etchant (BOE), e) photoresist stripping, f) oxygen plasma for bonding inlet and outlet-punched flat PDMS surfaces, g) the representative sketches of the two geometries of the microfluidic channels.

the photoresist coated glass slide with a light power of 160 mJ cm^{-2}. After that, the developing step was done by using AZ400K Dev 1:4 as the developer solution for 1 min and 20 s. The photoresist was hard baked at 110 °C lasting for 1 h and 30 min. The patterned glass slide was naturally cooled down to room temperature before wet etching and equilibrated for at least 2 h. After making sure that it reached room temperature, the glass slide was placed vertically in a PTFE container filled with BOE 7:1 solution and etched in an ultrasonic bath for 20 min. The channel depth was measured with a scanning electron microscope and a confocal microscope as 14 µm under these conditions. For deeper channels, the duration of the wet etching step was modified such that ≈700 nm min^{-1} of etch rate was present (appeared to be linear for at least 30 min of etching). It was found that for the edges of the pattern to be etched smoothly, the temperature should not exceed 27 °C during the wet etching process. After etching, the glass slides were rinsed with pure water in two steps and were placed in acetone for photoresist stripping without allowing the surface to dry. The stripping was done again in an ultrasonic bath for 10 min. Afterward, the channel-etched slides were rinsed with copious amounts of acetone, pure water, and isopropyl alcohol without drying to remove any residues from glass surfaces. Lastly, the slides were dried and became ready for use PDMS bonding.

The polydimethylsiloxane (PDMS) was prepared by mixing base and curing agent in a 10:1 mass ratio for 5 min to ensure complete mixing of the two parts. The mixture was placed into a vacuum desiccator for 30 min with a continuously applied vacuum to remove the bubbles. Flat PDMS cover pieces were prepared with aluminum foil and OTS coated glass slides (OTS was deposited in a vacuum chamber for at least 30 mins beforehand). The transparent PDMS mixture was poured into the molds and cured at 60 °C for 2 h in an oven. They were cooled down to room temperature. Appropriate sizes of PDMS to cover the microfluidic channels were cut from the mold, and inlet and outlet holes were punched using a 1.5 mm-sized biopsy punch. The prepared PDMS was rinsed with IPA (isopropyl alcohol) and dried. Oxygen plasma (Diener Electronics, Ebhausen, Germany) was used to activate the surfaces of the PDMS and the channel-etched glass slides for bonding. The glass slides and PDMS were placed into the chamber and vacuumed for 2 min. Then, oxygen was introduced to the system for 30 s. The plasma was applied for 20 s. After ventilation glass slide and PDMS were bonded by gently contacting each other, considering the alignment of the inlet and outlet holes. The platform was ready to use after connecting the 1.5 mm PTFE tubing of the inlet materials (connected to a microfluidic flow system, ElveFlow, OB1 controller).

Surface treatment of the microchannels: Microfluidic pressure-driven pumps (ElveFlow, Paris, France) were used to create flow inside microfluidic channels. Pure water was fed to the microfluidic channel platform for at least 10 min initially. From one side of the channel, 1% by volume of aqueous DMOAP solution was introduced to functionalize one side of the main channel with hydrophobic groups. It must be underlined that the path that DMOAP solution flows must be functionalized homogeneously for stable virtual walls between the LC and aqueous phases. The preferred procedure where a stable interface was obtained during experiments was functionalizing at 150 mbar inlet pressure for at least 15 min by flowing with water side-by-side. After the flow of the DMOAP solution, the DMOAP solution inlet tubing was removed gently, and the channel was rinsed with pure water for at least 15 min. 4-Cyano-4-pentylbiphenyl (5CB) flow was started without removing water from the other inlet (or without drying the channel to eliminate potential contamination and loss of hydrophilicity). The soft interface was formed as 5CB was going further along the channel. The microfluidic flow experiments were conducted at room temperature.

Microscopy: Images were collected by using Zeiss LSM 900 (Zeiss, Jena, Germany) equipped with a rotatable linear polarizer and analyzer. The polarizer and analyzer were arranged in either 45°–135° or 0°–90° pairs with respect to the main channel axis during transmission-mode polarized optical microscopy characterization as indicated in the figures. Fluorescence confocal polarizing microscopy (FCPM) techniques were used to distinguish how LC mesogens aligned along the channel by collecting confocal images to understand 3D structure. The fluorescent Nile Red dye (λ_{ex} = 549 nm, λ_{em} = 628 nm) was preferred for confocal imaging since it allows the determination of the local molecular alignment of the

LC mesogens.[51,52] A 0.01% by weight mixture of Nile Red in 5CB was prepared for imaging. The z-stack experiments were conducted with the values of 2.0% intensity of 561 nm laser, 750 V master gain, and 78 µm pinhole, with a 40x lens.

Velocity Measurements: The flow velocities in the microchannel were measured by particle tracking of the particles dispersed in 5CB. Average velocities were matched to the pressures set. Then, the relationship between the angle of the director of LC mesogens and the velocity was established (details of such methods are described elsewhere[45,53]).

Contact angle and Interfacial Tension Measurements: Contact angle measurements were done with DataPhysics OCA 200 model goniometer (DataPhysics Instruments, Filderstadt, Germany) advancing and receding angles were obtained by the needle-in method, in pure water with the glass slides with surfaces modified, similar to match the experimental conditions. Interfacial tension measurements were done using the same goniometer with the pendant drop method.

Statistical Analysis: The sample sizes (n) and error bars are defined in the text when needed. The data were reported as mean ± standard deviation.

Supporting Information

Supporting Information is available from the Wiley Online Library or from the author.

Acknowledgements

Conflict of Interest

The authors declare no conflict of interest.

Data Availability Statement

All raw data supporting the findings of this study are openly available on zenodo.org.

Keywords

[1] P. G. de Gennes, J. Prost, *The Physics of Liquid Crystals*, 2nd, Oxford University Press, New York, USA **1995**.

[2] E. Bukusoglu, M. A. Bedolla-Pantoja, P. C. Mushenheim, X. Wang, N. L. Abbott, *Annu. Rev. Chem. Biomol. Eng.* **2016**, *7*, 163.

[3] I. Lin, D. S. Miller, P. J. Bertics, C. J. Murphy, J. J. de Pablo, N. L. Abbott, *Science* **2011**, *332*, 1297.

[4] Y. K. Kim, X. Wang, P. Mondkar, E. Bukusoglu, N. L. Abbott, *Nature* **2018**, *557*, 539.

[5] P. Beyazkilic, S. Akcimen, C. Elbuken, B. Ortaç, S. Cai, E. Bukusoglu, *Adv. Funct. Mater.* **2022**, *32*, 12.

[6] X. Wang, H. Sun, Y. K. Kim, D. B. Wright, M. Tsuei, N. C. Gianneschi, N. L. Abbott, *Adv. Mater.* **2022**, *34*, 12.

[7] X. Wang, J. Krishna, A. Fernandez, S. Thayumanavan, N. L. Abbott, *Langmuir* **2023**, *39*, 1793.

[8] X. Wang, D. S. Miller, E. Bukusoglu, J. J. de Pablo, N. L. Abbott, *Nat. Mater.* **2016**, *15*, 106.

[9] F. Mukherjee, A. Shi, X. Wang, F. You, N. L. Abbott, *Small* **2023**, *19*, 2207802.

[10] J. A. Moreno-Razo, E. J. Sambriski, N. L. Abbott, J. P. Hernández-Ortiz, J. J. De Pablo, *Nature* **2012**, *485*, 86.

[11] Y. K. Kim, J. Noh, K. Nayani, N. L. Abbott, *Soft Matter* **2019**, *15*, 6913.

[12] D. S. Miller, X. Wang, N. L. Abbott, *Chem. Mater.* **2014**, *26*, 496.

[13] D. Seč, S. Čopar, S. Žumer, *Nat. Commun.* **2014**, *5*, 3057.

[14] A. Sengupta, U. Tkalec, C. Bahr, *Soft Matter* **2011**, *7*, 6542.

[15] A. Sengupta, U. Tkalec, M. Ravnik, J. M. Yeomans, C. Bahr, S. Herminghaus, *Phys. Rev. Lett.* **2013**, *110*, 048303.

[16] A. Sengupta, C. Bahr, S. Herminghaus, *Soft Matter* **2013**, *9*, 7251.

[17] V. M. O. Batista, M. L. Blow, M. M. Telo Da Gama, *Soft Matter* **2015**, *11*, 4674.

[18] T. Emeršič, R. Zhang, Ž. Kos, S. Čopar, N. Osterman, J. J. de Pablo, U. Tkalec, *Sci. Adv.* **2019**, *5*, eaav4283.

[19] S. Čopar, Ž. Kos, T. Emeršič, U. Tkalec, *Nat. Commun.* **2020**, *11*, 59.

[20] A. Sengupta, B. Schulz, E. Ouskova, C. Bahr, *Microfluid. Nanofluidics* **2012**, *13*, 941.

[21] A. Sengupta, S. Herminghaus, C. Bahr, *Liq. Cryst. Rev.* **2014**, *2*, 73.

[22] H. Agha, C. Bahr, *Soft Matter* **2016**, *12*, 4266.

[23] H. Agha, C. Bahr, *Soft Matter* **2018**, *14*, 653.

[24] G. A. Vásquez-Montoya, T. Emeršič, N. Atzin, A. Tavera-Vázquez, A. Mozaffari, R. Zhang, O. Guzmán, A. Snezhko, P. F. Nealey, J. J. de Pablo, *Soft Matter* **2024**, *20*, 397.

[25] C. J. Holmes, S. L. Cornford, J. R. Sambles, *Phys. Rev. Lett.* **2010**, *104*, 248301.

[26] K. Fedorowicz, R. Prosser, *Sci. Rep.* **2024**, *14*, 4875.

[27] Q. Zhang, W. Wang, S. Zhou, R. Zhang, I. Bischofberger, *Nat. Commun.* **2024**, *15*, 7.

[28] O. Wiese, D. Marenduzzo, O. Henrich, *Soft Matter* **2016**, *12*, 9223.

[29] S. Roh, M. Tsuei, N. L. Abbott, *Langmuir* **2021**, *37*, 5810.

[30] S. Maiti, S. Roh, I. Cohen, N. L. Abbott, *J. Colloid Interface Sci.* **2023**, *637*, 134.

[31] H. A. Fuster, X. Wang, X. Wang, E. Bukusoglu, S. E. Spagnolie, N. L. Abbott, *Sci. Adv.* **2020**, *6*, eabb1327.

[32] A. Akman, E. Bukusoglu, *J. Colloid Interface Sci.* **2023**, *649*, 772.

[33] B. Zhao, J. S. Moore, D. J. Beebe, *Science* **2001**, *291*, 1023.

[34] B. Zhao, J. S. Moore, D. J. Beebe, *Anal. Chem.* **2002**, *74*, 4259.

[35] J. Atencia, D. J. Beebe, *Nature* **2005**, *437*, 648.

[36] A. Aota, K. Mawatari, T. Kitamori, *Lab Chip* **2009**, *9*, 2470.

[37] A. Aota, A. Hibara, T. Kitamori, *Anal. Chem.* **2007**, *79*, 3919.

[38] A. Aota, M. Nonaka, A. Hibara, T. Kitamori, *Angew. Chemie* **2007**, *119*, 896.

[39] M. Tokeshi, T. Minagawa, K. Uchiyama, A. Hibara, K. Sato, H. Hisamoto, T. Kitamori, *Anal. Chem.* **2002**, *74*, 1565.

[40] A. Hibara, S. Iwayama, S. Matsuoka, M. Ueno, Y. Kikutani, M. Tokeshi, T. Kitamori, *Anal. Chem.* **2005**, *77*, 943.

[41] A. Hibara, M. Nonaka, H. Hisamoto, K. Uchiyama, Y. Kikutani, M. Tokeshi, T. Kitamori, *Anal. Chem.* **2002**, *74*, 1724.

[42] C. Poulard, M. Voué, J. De Coninck, A. M. Cazabat, *Colloids Surfaces A Physicochem. Eng. Asp.* **2006**, *282*, 240.

[43] S. Şengül, N. Aydoğan, E. Bukusoglu, *J. Colloid Interface Sci.* **2022**, *608*, 2310.

[44] S. A. Jewell, S. L. Cornford, F. Yang, P. S. Cann, J. R. Sambles, *Phys. Rev. E.* **2009**, *80*, 041706.

[45] D. S. Miller, R. J. Carlton, P. C. Mushenheim, N. L. Abbott, *Langmuir* **2013**, *29*, 3154.

[46] N. A. Lockwood, J. K. Gupta, N. L. Abbott, *Surf. Sci. Rep.* **2008**, *63*, 255.

[47] I. I. Smalyukh, *Mol. Cryst. Liq. Cryst.* **2007**, *477*, 23/[517].

[48] J. K. Gupta, N. L. Abbott, *Langmuir* **2009**, *25*, 2026.

[49] K. Nayani, P. Rai, N. Bao, H. Yu, M. Mavrikakis, R. J. Twieg, N. L. Abbott, *Adv. Mater.* **2018**, *30*, 1706707.

[50] R. U. Dinc, E. Bukusoglu, *Soft Matter* **2023**, *19*, 4304.

[51] I. I. Smalyukh, S. V. Shiyanovskii, O. D. Lavrentovich, *Chem. Phys. Lett.* **2001**, *336*, 88.

[52] H. Tajalli, A. G. Gilani, M. S. Zakerhamidi, P. Tajalli, *Dye. Pigment.* **2008**, *78*, 15.

[53] S. C. Zhao, C. L. Yuan, Y. F. Wang, P. Z. Sun, B. H. Liu, H. L. Hu, D. Shen, Z. G. Zheng, *J. Mater. Chem. C* **2022**, *10*, 11767.